A Finite Element Projection Method for Low-Mach Number Reacting Flows

Mark A. Christon

Sandia National Laboratories, Computational Physics R&D,

Albuquerque, NM 87185, USA

Ranjeet S. Patil

University of New Mexico, Mechanical Engineering Department,

Albuquerque, NM 87131, USA

Abstract

We extend the optimal second-order finite element projection method developed by Gresho and Chan[1] in order to treat low-Mach number reacting flows using simple/reduced-order chemistry. The reacting flow formulation considers the zero Mach-number limit for combustion allowing for large heat release and the concomitant excursions in temperature and density while avoiding the need for a fully-compressible numerical treatment. In order to avoid spurious oscillations due to non-smooth data, a flux-corrected advection algorithm based on an explicit predictor/semi-implicit corrector and characteristic-based limiting is used. Results are presented for variable density non-reacting/reacting wakes and illustrate the process of bluff-body flame stabilization.

Keywords: low-Mach number; reacting flow, finite element; projection method; CFD

1 Introduction

The incompressible/low-Mach number flow regime spans a spectrum of applications ranging from vehicle aerodynamics and flow-induced noise to mold-filling and chemically reacting flows. In this work, we extend Gresho and Chan's optimal second-order projection method[1] to treat low-Mach number reacting flows.

The low-Mach number regime is observed in devices such as pumps, burners, internal combustion engines (under normal operating conditions), and CVD reactors. In low-Mach number flows, the pressure remains nearly constant in space and exhibits only small excursions about the mean pressure. Acoustic waves in such flows are typically weak, contain a small fraction of the kinetic energy, and equilibrate rapidly.

We begin with the simplified reacting flow formulation by Majda and Sethian[2] in which the effects of acoustic waves are removed. As demonstrated by Lai[3, 4] this approach yields a computational advantage over a fully-compressible treatment that scales roughly as the inverse of the Mach number, i.e., $1/M$. We also note in passing the acoustically-filtered low-Mach formulation is not new and has been used by many other researchers, e.g., see Paolucci[5] and Martinez[6].

For our purposes, we assume a premixed fuel with only two species present – un-burnt and burnt gas. Both the reactants and products are assumed to follow the same γ-law equation of state and have similar molecular weights. Reactions occur via single-step irreversible Arrhenius chemical kinetics. Although the effects of acoustic waves have been filtered from the governing equation, the formulation admits large excursions in temperature and density consistent with large heat release due to chemical reactions.

In the following section, a brief overview of the formulation and numerical method is presented. This is followed by computational results that demonstrate the extended projection method for variable-density non-reacting and reacting wakes flows. Finally, a summary and conclusions are presented.

2 Formulation

We consider a flow domain Ω with boundary $\Gamma = \Gamma_1 \bigcup \Gamma_2$. In the low-Mach number limit, the pressure can be segregated into a bulk thermodynamic part, $\bar{p}(t)$, and a "kinematic" part, $p(\mathbf{x}, t)$, as $\hat{p}(\mathbf{x}, t) = \bar{p}(t) + p(\mathbf{x}, t)$. In the incompressible limit, $\nabla \cdot \mathbf{u} = 0$, the kinematic pressure plays the role of a Lagrange multiplier.

Conservation of species, energy and linear momentum for the reacting flow system are

$$\rho \left\{ \frac{\partial Z}{\partial t} + u \cdot \nabla Z \right\} = \nabla \cdot (\rho \mathcal{D} \nabla Z) - k \rho Z \tag{1}$$

$$\rho C_p \left\{ \frac{\partial T}{\partial t} + u \cdot \nabla T \right\} = \frac{d\bar{p}}{dt} + \nabla \cdot \kappa \nabla T + q_0 \rho k Z + q''' \tag{2}$$

$$\rho \left\{ \frac{\partial \mathbf{u}}{\partial t} + (\mathbf{u} \cdot \nabla)\mathbf{u} \right\} = -\nabla p + \nabla \cdot [\mu(\nabla \mathbf{u} + (\nabla \mathbf{u})^T)] + \mathbf{f} \tag{3}$$

where ρ is the mass density, $\mathbf{u}$ the velocity, T the temperature, and Z the mass fraction of the reactants. Fluid properties consist of μ the viscosity, C_p the constant-pressure specific heat, κ the thermal conductivity, and $\mathcal{D}$ the species diffusivity. A body force $\mathbf{f}$ is included in the momentum equations, and in the energy equation, q_0 is the reaction-rate heat release coefficient, $k = A \exp\left(-\frac{E}{RT}\right)$ the reaction rate, and q''' the volumetric heat source.

The equation of state is $\rho = \bar{p}/RT$, where $R = C_p/C_v$ is the ratio of the specific heats, and the rate equation for the thermodynamic pressure is,

$$\frac{d\bar{p}}{dt} = \frac{(\gamma - 1)}{V_{Tot}} \int_{\Omega} (q_0 k \rho Z + \nabla \cdot \kappa \nabla T) d\Omega. \tag{4}$$

where V_{Tot} is the total domain volume. Combining energy, mass conservation, and using Eq.(4), a div-constraint is constructed as

$$\nabla \cdot \mathbf{u} = \frac{1}{\gamma \bar{p}} \left\{ -\frac{d\bar{p}}{dt} + (\gamma - 1)(q_0 k \rho Z + \nabla \cdot \kappa \nabla T) \right\}. \tag{5}$$

Boundary conditions for the system include specified velocity, temperature and species conditions on Γ_1, and specified traction boundary conditions, heat and mass fluxes on Γ_2. Initial conditions consist of prescribed velocity, temperature and species distributions, $\mathbf{u}(\mathbf{x}, 0) = \mathbf{u}_0(\mathbf{x})$, $T(\mathbf{x}, 0) = T_0(\mathbf{x})$, $Z(\mathbf{x}, 0) = Z_0(\mathbf{x})$. The initial thermodynamic pressure is specified, and the density computed as $\rho_0(\mathbf{x}) = \bar{p}_0/RT_0(\mathbf{x})$.

The numerical solution method is based on the Galerkin finite element method with several modifications that include pressure stabilization, balancing tensor diffusivity for second-order temporal accuracy in the explicit advection, and linearization of the mass and energy reaction rate terms. An explicit forward-Euler predictor is used in conjunction with a trapezoidal-rule correction for the overall system of equations. Due to space limitations, we omit the details of the forward-Euler predictor, and begin with the species transport equation, using predicted values of density $\tilde{\rho}^{n+1}$ and reaction rate $\tilde{k}^{n+1}$,

$$\begin{aligned} &\left[\bar{M} + \theta \Delta t \left(\tilde{K}_Z + \mathcal{R}(1, \tilde{\rho}^{n+1}, \tilde{k}^{n+1})\right)\right] Z^{n+1} = \\ &\quad \Delta t[(1-\theta)\dot{m}^n + \theta \dot{m}^{n+1}] + \\ &\quad \left[\bar{M} - \Delta t(1-\theta)\left(\tilde{K}_Z - \mathcal{R}(1, \rho^n, k^n)\right)\right] Z^n - \Delta t A(\rho^n, \mathbf{u}^n) Z^n. \end{aligned} \tag{6}$$

Here, $\mathcal{R}(\cdot,\rho,\cdot)$ is a generalized reaction-rate operator that accepts as arguments a heat release rate, density, and linearized reaction rate. $A(\cdot,\cdot)$ is a generalized advection operator, $\tilde{K}_Z$ is the mass diffusion operator evaluated at $n+1/2$, and $\bar{M}$ is the mass matrix evaluated using $\bar{\rho} = (\rho^n + \tilde{\rho}^{n+1})/2$. $\dot{m}$ represents additional mass source/sinks. The choice of time-centering in $\mathcal{R}(\cdot,\rho,\cdot)$ is made to ensure stable ODE's given $0 \leq Z \leq 1$.

The energy equation corrector is,

$$\begin{aligned}
&\left[\bar{M}_T + \theta\Delta t\left\{\tilde{K}_T - \mathcal{R}\left(q_0, \tilde{\rho}^{n+1}, \left(\frac{\partial k}{\partial T}\right)^n\right) Z^{n+1}\right\}\right] T^{n+1} = \\
&\quad \Delta t[(1-\theta)Q^n + \theta Q^{n+1}] + \\
&\quad \Delta t(1-\theta)[\dot{\bar{p}}^n M_L^u + \mathcal{R}\left(q_0, \rho^n, k^n\right) Z^n] + \\
&\quad \Delta t\theta[\dot{\bar{p}}^{n+1} M_L^u + \mathcal{R}\left(q_0, \tilde{\rho}^{n+1}, k^n\right) Z^{n+1}] + \\
&\quad \left[\bar{M}_T - \Delta t(1-\theta)\left\{\tilde{K}_T - \mathcal{R}\left(q_0, \rho^n, \left(\frac{\partial k}{\partial T}\right)^n\right) Z^{n+1}\right\}\right] T^n - \Delta t A(\rho^n, \mathbf{u}^n) T^n, \qquad (7)
\end{aligned}$$

where $\bar{M}_T$ is the thermal capacitance matrix computed using $\bar{\rho}$ and C_p. M_L^u is a unit row-sum lumped mass matrix.

The momentum corrector is,

$$\begin{aligned}
&\left[\bar{M} + \theta\Delta t\tilde{K}^{n+1/2}\right] \tilde{\mathbf{u}}^{n+1} = \\
&\quad \Delta t\left[(1-\theta)\mathbf{F}^n + \theta\mathbf{F}^{n+1} - A(\rho^n, \mathbf{u}^n)\mathbf{u}^n - [\bar{M}\bar{M}_L^{-1}]CP^n\right] \\
&\quad \left[\bar{M} - (1-\theta)\Delta t\tilde{K}^{n+1/2}\right] \mathbf{u}^n. \qquad (8)
\end{aligned}$$

The thermodynamic pressure is

$$\begin{aligned}
&\bar{p}^{n+1}\left[1 - \theta\Delta t\left\{q_0\frac{(\gamma-1)}{V_{T_0 t}}\sum_{i=1}^{Nnp}\left[\mathcal{R}\left(\frac{1}{RT^{n+1}}, 1, k^{n+1}\right) Z^{n+1}\right]_i\right\}\right] = \\
&\quad \Delta t(1-\theta)\left\{q_0\frac{(\gamma-1)}{V_{T_0 t}}\sum_{i=1}^{Nnp}\left[\mathcal{R}(1, \rho^n, k^n) Z^n\right]_i\right\}, \qquad (9)
\end{aligned}$$

where Nnp is the number of nodes in the mesh.

In order to avoid non-physical oscillations due to steep gradients and reaction source terms, a non-linear, characteristic-based, monotonicity-preserving advection algorithm motivated by flux-corrected transport (FCT)[7, 8, 9] has been developed. An explicit advection-only step is used as the low-order predictor with an "operator" limiting procedure based on preserving monotonicity. The limiting is based on values obtained by examining advective field values in the backward characteristic direction as shown in Figure 1(a). Once the limited operator is obtained, $A(\cdot, \cdot)$, a semi-implicit corrector is used to advance the solution in time.

The monotonicity-preserving advection treatment is demonstrated using a $Re = 4000$ time-dependent, heated, momentum-driven jet. Figure 1(b) shows temperature-time history points during the startup phase with a $100K$ step-change in the initial temperature field. Figure 1(c) shows a snapshot of the temperature field for the heated jet relative to the time-history points. The advective treatment preserves the fourth-order phase accuracy of the finite element method and does not introduce excessive cross-stream diffusion as demonstrated by the sharp change in temperature at the base of the starting jet, and the formation of the Kelvin-Helmholtz shear layer shown later in time in Figure 1(d).

3 Results

This section summarizes results of computations carried out for reacting and non-reacting wake flows behind a cylinder. Initial time-accurate computations were carried out for a $Re = 100$, $Sc = 1$ flow past a circular cylinder for the non-reacting case using a steady

parabolic inlet velocity profile with no-slip, no-penetration boundary conditions imposed on the cylinder, upper and lower walls. A constant non-dimensional temperature boundary condition is applied at the cylinder wall. At $t = 1$ a steady mass concentration $Z = 1$ is prescribed at the upstream boundary.

Figure 2 shows snapshots of the temperature, mass fraction, z-vorticity, and pressure field during the vortex-shedding cycle for the non-reacting case. In contrast, Figure 3 shows a snapshot at the same point during the shedding cycle for the reacting case. Here, the differences in the wake are most clearly identified in the temperature and mass fraction.

In ramjet and turbojet combustors, the flow velocities are sufficiently high relative to the flame speed that it is necessary to provide some sort of flame stabilization. This is typically done by inserting a bluff-body in the flow causing recirculation and resulting in a continuous ignition of the air-fuel mixture (see for example Glassman[10] pp. 206 – 215). A prototype calculation to illustrate the effect of bluff-body stabilization on a vortex street was carried out for $Re = 1000$. Here, the conditions were similar to the $Re = 100$ calculations, but a cylinder temperature of 1000 K was imposed. Figure 4 (a) shows snapshots of the temperature, mass species and density during the initial vortex-shedding phase. In Figure 4 (b), a snapshot of the fields is presented after the wake has begun to stabilize. Note the formation of a nearly symmetric wake behind the cylinder and the absence of any coherent Karman vortex street after approximately 1.35 seconds – or ~ 5 isothermal shedding cycles.

4 Summary & Conclusions

A new finite element projection method for treating the simplified low-Mach reacting flow equations which is based on extensions to Gresho and Chan's optimal second-order projection method has been presented. A new time-dependent flux-correction technique for monotonicity preserving advection has been introduced and successfully applied to chemically reacting flows. The extended projection method has been demonstrated to be stable and robust for relatively high Reynolds number reacting flows. The extension to more complex chemistry with multiple species appears to be feasible in the current projection-based computational framework.

References

[1] Philip M. Gresho and Stevens T. Chan. On the theory of semi-implicit projection methods for viscous incompressible flow and its implementation via a finite element method that also introduces a nearly consistent mass matrix. part 2: Implementation. *International Journal for Numerical Methods in Fluids*, 11:621–659, 1990.

[2] Andrew Majda and James Sethian. The derivation and numerical solution of the equations for zero mach number combustion. *Combustion Science and Technology*, 42:185–205, 1985.

[3] Mindy Fruchtman Lai. *A Projection Method for Reacting Flow in the Zero Mach Number Limit*. PhD thesis, University of California at Berkeley, 1993.

[4] Mindy Lai, John B. Bell, and Phillip Colella. A projection method for combustion in the zero mach number limit. In *Eleventh AIAA Computational Fluid Dynamics Conference*, pages 776–783. AIAA, 1993.

[5] S. Paolucci. On the filtering of sound from the navier-stokes equations. Technical Report SAND82-8257, Sandia National Laboratories, December 1982.

[6] M. J. Martinez. Analysis of anelastic flow and numerical treatment via finite elements. Technical Report SAND94-0320, Sandia National Laboratories, May 1994.

[7] Jay P. Boris and David L. Book. Flux corrected transport I: SHASTA, a fluid transport algorithm that works. *Journal of Computational Physics*, 11:38–69, 1973.

[8] David L. Book, Jay P. Boris, and K. Hain. Flux corrected transport II: Generalizations of the method. *Journal of Computational Physics*, 18:248–283, 1975.

[9] Jay P. Boris and David L. Book. Flux corrected transport III: minimal-error FCT algorithms. *Journal of Computational Physics*, 20:397–431, 1976.

[10] I. Glassmann. *Combustion.* Academic Press, San Diego, California, third edition, 1996.

Figure 1: Advective treatment demonstrated using a $Re = 4000$ heated, momentum-driven jet: (a) Characteristic-based limiting, (b) Temperature time histories at nodes 10, 26 and 50, (c) Snapshot of starting momentum-driven jet at $t = 0.15$, (d) Snapshot of temperature after the onset of the Kelvin-Helmholtz shear instability.

Figure 2: Non-reacting wake (a) Temperature, (b) Mass Fraction, (c) Vorticity, (d) Pressure.

Figure 3: Reacting wake showing (a) Temperature, (b) Mass Fraction, (c) Vorticity, (d) Pressure.

Figure 4: $Re = 1000$ reacting wake (a) Snapshot at $t = 2.39$s, (b) Initiation of bluff-body stabilization at $t = 3.75$s.

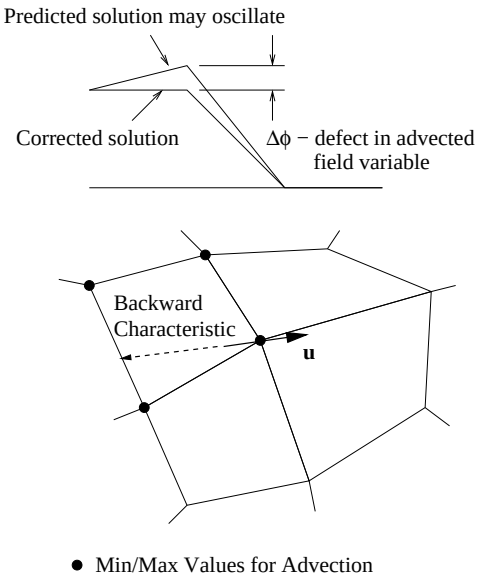

(a)

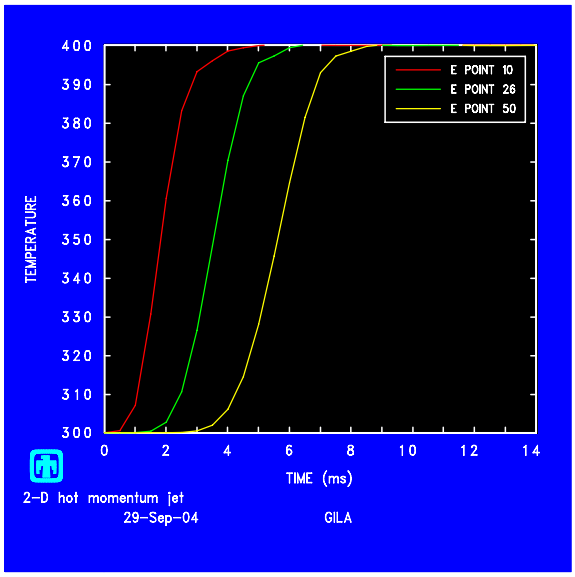

(b)

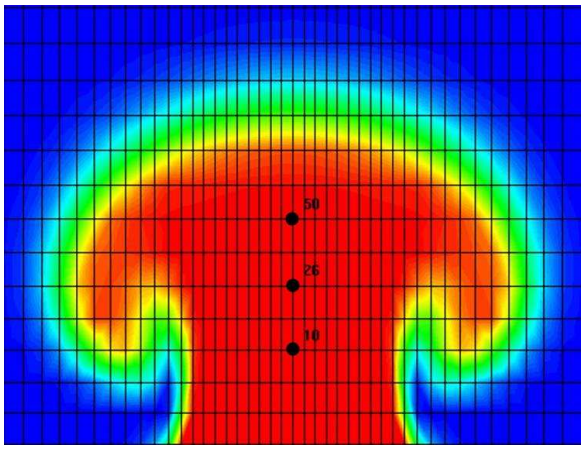

(c)

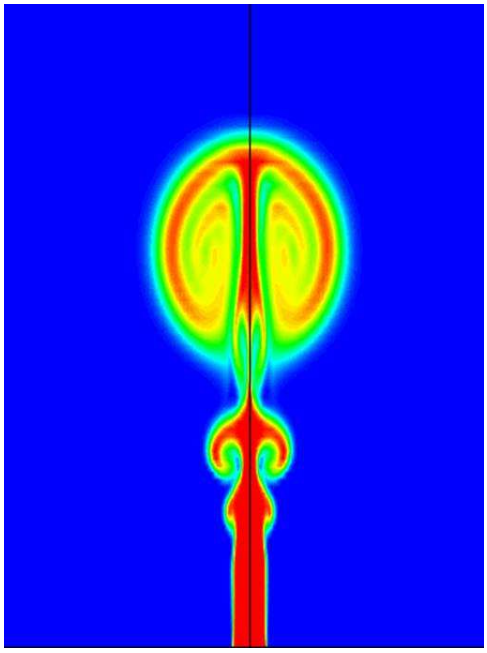

(d)

Figure 1:

(a)

(b)

(c)

(d)

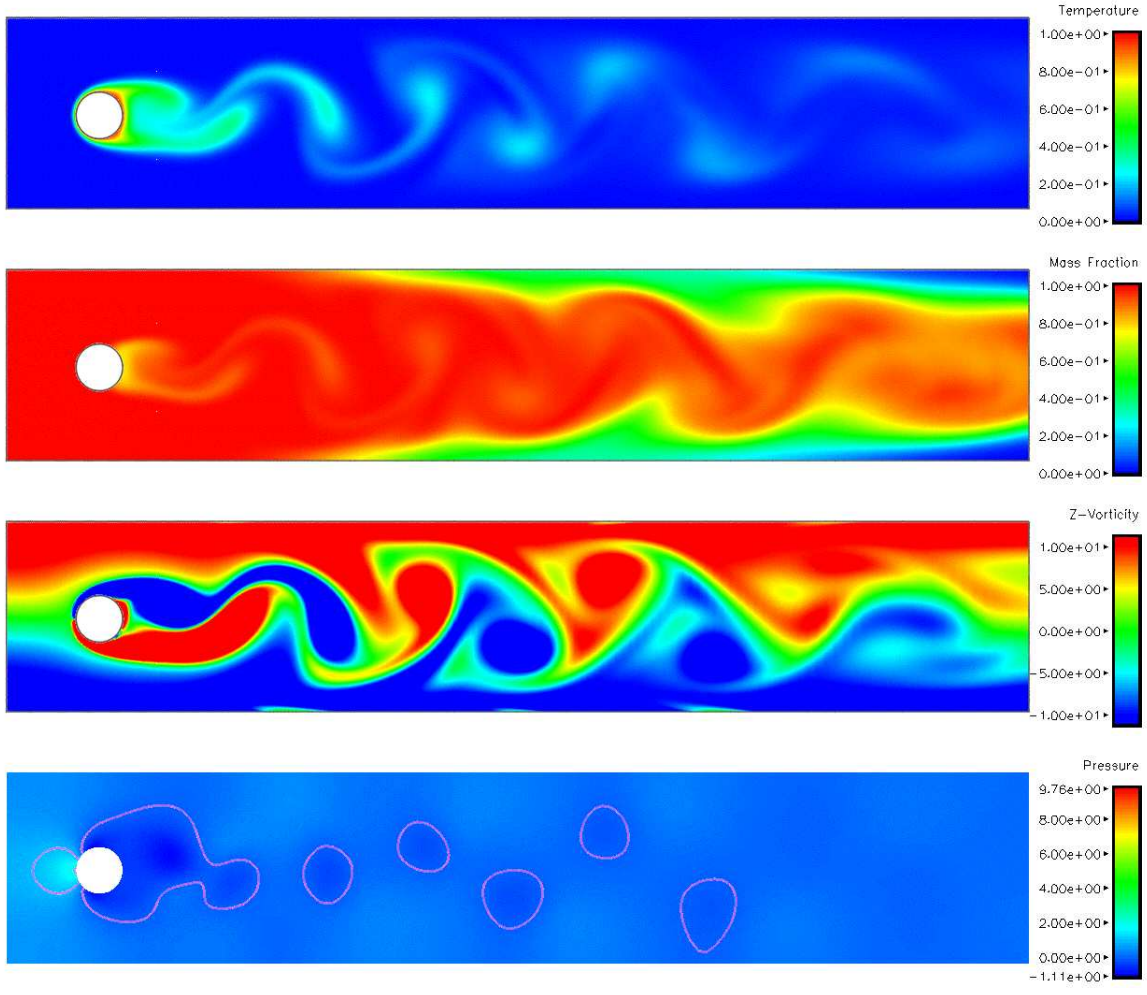

Figure 2:

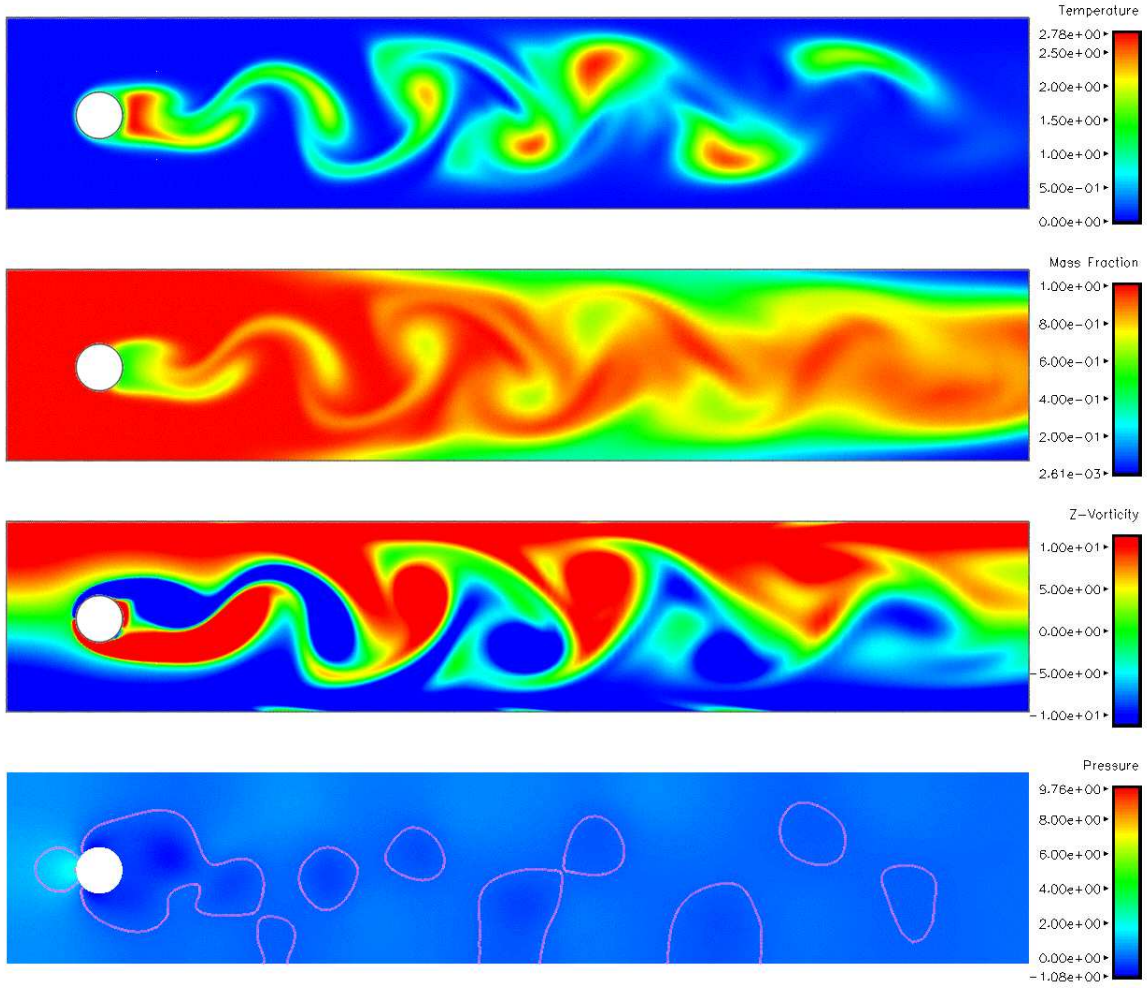
(a)
Temperature
2.78e+00
2.50e+00
2.00e+00
1.50e+00
1.00e+00
5.00e-01
0.00e+00
(b)
Mass Fraction
1.00e+00
8.00e-01
6.00e-01
4.00e-01
2.00e-01
2.61e-03
(c)
Z-Vorticity
1.00e+01
5.00e+00
0.00e+00
-5.00e+00
-1.00e+01
(d)
Pressure
9.76e+00
8.00e+00
6.00e+00
4.00e+00
2.00e+00
0.00e+00
-1.08e+00

Figure 3:

(a)

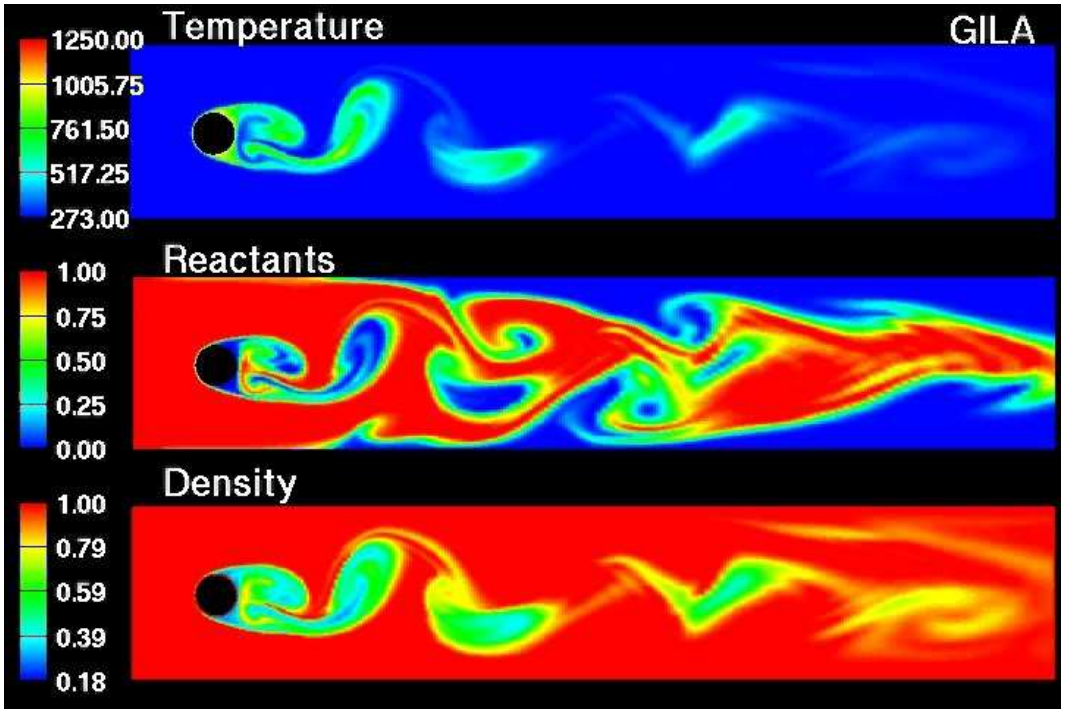
Temperature
GILA
1250.00
1005.75
761.50
517.25
273.00
Reactants
1.00
0.75
0.50
0.25
0.00
Density
1.00
0.79
0.59
0.39
0.18

(b)

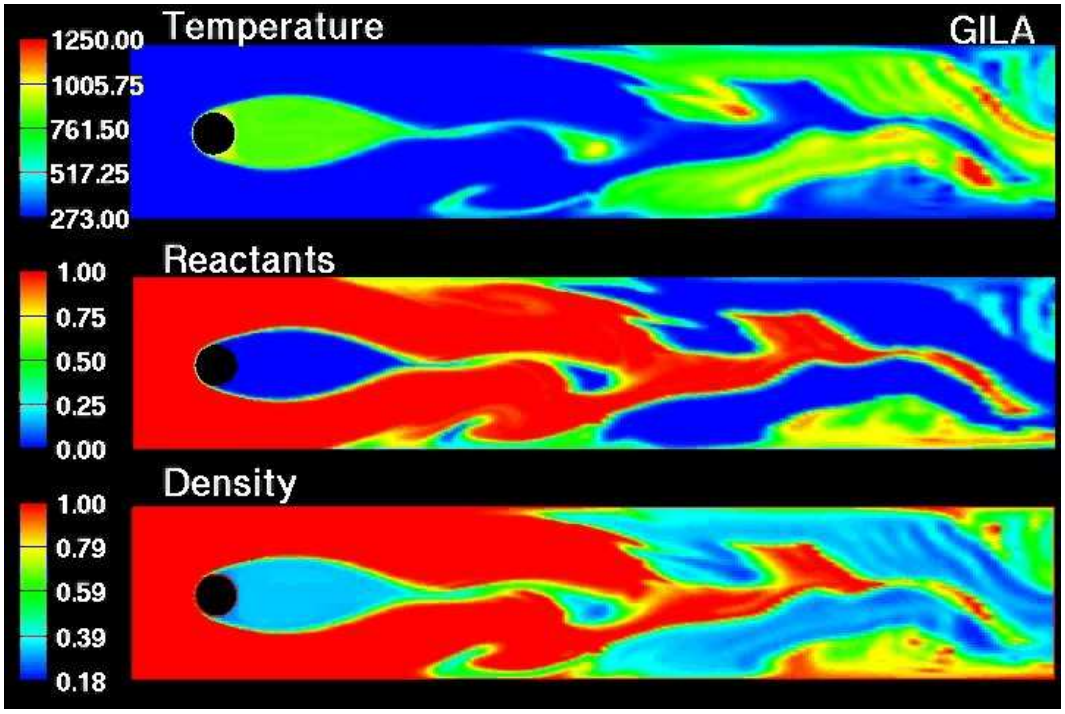
Temperature
GILA
1250.00
1005.75
761.50
517.25
273.00
Reactants
1.00
0.75
0.50
0.25
0.00
Density
1.00
0.79
0.59
0.39
0.18

Figure 4: